CMS Methods for Efficient Damping Prediction for Structures with Friction

Jens Becker and Lothar Gaul
Institute of Applied and Experimental Mechanics, University of Stuttgart
Pfaffenwaldring 9, 70550 Stuttgart, Germany

Abstract

Friction in joints significantly contributes to the observed overall damping of mechanical structures. Especially if the material damping is low, the frictional effects in joints and clamping boundary conditions dominate the structural damping. The damping and the stiffness of the structure are nonlinear functions of the system states and consequently of the excitation signal and amplitude. If these nonlinear effects should be incorporated in the design process, transient simulations must be employed in order to predict and analyze the damping for a given excitation, though they need excessive computation power due to the nonlinear constitutive laws and the high contact stiffnesses.

As one approach to alleviate transient simulations, the application of component mode synthesis (CMS) methods to structures with friction is investigated exploiting the linearity of the jointed substructures. The nonlinear frictional effects and the normal contact is modeled by constitutive laws implemented in a zero–thickness–element formulation. The necessary considerations for accurate damping prediction by the reduced models, the accuracy and the computational times for transient simulations are presented. The found model reduction techniques allow a strong reduction of the computation time which in turn makes it a promising tool for model updating and predictive parameter studies. As an application example, a beam–like structure with attached friction damper is investigated in simulations and the obtained numerical results after model updating are compared to experiments.

Nomenclature

$\boldsymbol{x}, \boldsymbol{q}$	physical, generalized coordinate vector
$\boldsymbol{M}, \boldsymbol{K}, \hat{\boldsymbol{M}}, \hat{\boldsymbol{K}}$	mass and stiffness matrix, hat indicates reduced mass and stiffness matrices
$\boldsymbol{F}, \boldsymbol{B}_\mathsf{T}, \boldsymbol{B}_\mathsf{N}$	right–hand–side load vectors
$\boldsymbol{g}$, $\boldsymbol{g}_\mathsf{ref}$	gap vector, gap vector of reference solution
u_rel	relative displacement
$F_{\mathsf{N},1}, F_{\mathsf{N},2}$	normal forces applied by the left and right bolt
E, E_ref	strain energy, strain energy of reference solution
μ	friction coefficient
$c_{\mathsf{N},0}, c_{\mathsf{N},1}, c_\mathsf{T}$	stiffness parameters in normal and tangential direction
g_0, g_1	gap parameters for normal contact law
ω, f	angular frequency, frequency

1 Introduction

Most real–world engineering mechanical structures contain nonlinear elements, e.g. play, nonlinear springs and stiffnesses, or joints with nonlinear contact and friction effects. It is known from experiments that friction, mostly microslip effects, in joints contribute significantly to the overall structural damping in metal structures [6, 14, 13, 7]. Due to the nonlinearities, analysis must be conducted costly in time domain or with special methods such as harmonic balance methods [17, 14, 12]. This is often avoided by using linear stiffness and damping models for harmonic analysis in frequency domain [1]. By this, it is exploited that most nonlinearities are located on interfaces connecting substructures for model order reduction therewith enabling transient analysis with fair cost for engineering mechanical structures. For example, one application is closed–loop simulations of semi–active controllers for friction dampers with controlled normal forces [2].

Although many publications cover model reduction techniques for mechanical structures with isolated nonlinearities, e.g. using Krylov–mode based reduction [8] or using proper orthogonal decomposition (POD) methods [16], only few consider distributed nonlinearities. For the investigated structure, namely a beam with attached friction damper beam, friction and

contact nonlinearities act on the contact area between base structure and friction damper. Though the contact area is small compared to the overall structure dimensions, it can not assumed to be point–like.

In Gaul et. al. [8], Krylov reduction methods are employed to efficiently simulate the dynamics of a truss structure as a typical lightweight construction. The truss is equipped with adaptive friction joints that can be semi–actively controlled to damp out vibrations excited by a snap–back of the truss tip. Model reduction is applied for the simulation of the closed–loop behavior and for the design of appropriate observers. In the first step of the model reduction, the dominant modes of the structure are determined and retained by modal truncation. Then, Krylov modes are determined for the linear transfer functions between every discrete adaptive joint model and the controlled variables and added to the reduction base. By this technique, a strong reduction of the computation time is achieved as long as not too many nonlinear joints have to be considered which would strongly increase the number of transfer functions that must be separately treated. A strong disadvantage of this approach is that the dynamics of the whole structure can not be recovered from the reduced solution, i.e. the interesting output variables must be already determined before the reduction step is conducted. Qu [15] investigates model reduction techniques for finite–element (FE) models with local nonlinearities. He proposes an iterative procedure to calculate reduced mass matrices from Guyan reduction that improves the accuracy at higher frequencies without adding additional DOFs. For two test structures, nonlinear FRFs are calculated from time simulations and the harmonic balance method for the full–order models of 82 and 165 DOFs, respectively, and are compared to results from reduced models.

Witteven and Irschik [18] propose model reduction techniques specifically for structure with bolted joints. They model only the nonlinear normal contact in the bolted joints without consideration of frictional effects. A reduction method based on the Craig–Bampton reduction method applied to the whole structure is proposed that accounts for actio and reactio at the contact interface. It is important to note, that the method is formulated for the whole structure only and does not exploit that the structure is made up from different jointed substructures.

Jalali et al. [9] considered two beams connected by a rotational joint with friction that is modelled by a discrete nonlinear joint model. Their dynamic model is based on the first bending mode obtained from a linear case. For vibrations close to the one considered mode, the joint model parameters are identified from experimental data. Unfortunately, it is not tested if the chosen joint model and the identified parameters are able to capture the dynamical behavior at other resonance frequencies as well and the question how to replace the nonlinear elements by linear ones for the modal reduction is not discussed.

Segalman [16] proposed the use of Eigenmodes in addition to special discontinuous global vectors (either eigenvector sensitivities or so–called Milman–Chu vectors) in order to strongly accelerate convergence of a Galerkin reduction method for model reduction of medium–scale mechanical systems with localized nonlinearities. The method is demonstrated for a 11 degrees of freedom (DOF) system with 1-D friction nonlinearities with the system energy time evolution as performance criteria, for which superior convergence is shown if the proposed discontinuous vectors are used. Kappagantu and Feeny [10, 11] apply proper orthogonal decomposition (POD) methods to determine reduction bases from arbitrary time signals that are obtained from either measurements or simulations. However, such POD methods generally yield black-box models that give no insight into the internal physics and the reduction quality strongly depends on a representative selection of the excitation signals. Only the selected outputs can be recovered from the reduced model solution, which strongly restricts the range of applications of these methods.

In summary – to the opinion of the authors – there is a lack of research of model–driven reduction strategies for mechanical structures with friction that systematically exploits the separation of the overall structure into jointed substructures. Such strategies are developed and investigated in the following, where they are used to efficiently predict the contributed damping of bolted joints and frictional interfaces to the overall structural damping.

1.1 Basics Concepts of Component Mode Synthesis

Component Mode Synthesis (CMS) methods reduce the complexity of structural dynamics models leading to reduced simulation time and reduced memory requirements. The linear subsystem models – in most cases obtained from FE discretization – are reduced with special consideration of the interface degrees of freedom (DOFs) and for a given frequency range of interest in a first step. Then, the reduced substructure models are assembled to the overall structural dynamics that has significantly less degrees of freedom. After analysis of this reduced model, the solution is expanded and the original vector of the physical DOFs is recovered.

In the following, displacement–based CMS is performed, i.e. approximate solutions in a reduced subspace (the range of the rectangular matrix $\boldsymbol{\Theta}$) are sought in a Rayleigh-Ritz sense,

$$\boldsymbol{x} \approx \boldsymbol{\Theta}\, \boldsymbol{q} \tag{1}$$

where the vector $\boldsymbol{x}$ contains the N unknown physical displacements and rotations and the vector $\boldsymbol{q}$ the $m << N$ reduced model coordinates. The matrix $\boldsymbol{\Theta}$ is called the reduction base or Ritz vector base. Because some kind of modes are used for building the reduction base, it is often called modal base.

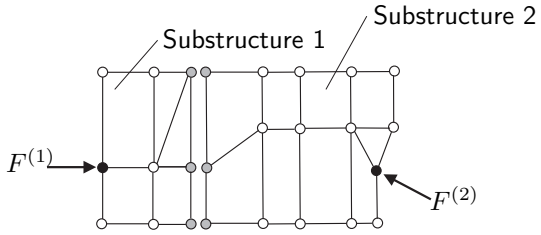

Figure 1: Sketch of two substructures with degrees of freedom (DOF) marked according to Tab. 1.

Table 1: Definition of degrees of freedom (DOF) vectors according to Fig. 1.

Variable	Name	Description
$\boldsymbol{x}_\mathsf{j}$	joint interface DOFs (gray)	joint interfaces DOFs of substructure 1 and substructure 2
$\boldsymbol{x}_\mathsf{j}^{(k)}$	joint k interface DOFs (gray)	joint interface DOFs of substructure k
$\boldsymbol{x}_\mathsf{f}^{(k)}$	free DOFs (white)	inner DOFs of substructure k
$\boldsymbol{x}_\mathsf{l}^{(k)}$	load DOFs (black)	DOFs of substructure k where external loads are applied

Typical methods combine normal modes of components obtained by different imposed boundary conditions at the interfaces (free, fixed or mass–loaded) and static modes from the static solution for applied interface loads (attachment modes) or imposed boundary displacement (constraint modes). Generally, the selection of the appropriate reduction base is performed in view of linear independence and completeness, low computational expense in their generation, automatic selection of their number and good convergence of the obtained solution to the exact (full) solution [3]. In the following, two model reduction techniques are derived using the nomenclature given in Tab. 1 and Fig. 1. Linear substructure models are assumed, i.e. small deformations and linear elasticity.

2 CMS Methods for Structures with Friction

In the following, a structure consisting of two connected substructures with friction in the contact interface is considered,

$$\underbrace{\begin{bmatrix}\boldsymbol{M}^{(1)} & \boldsymbol{0}\\ \boldsymbol{0} & \boldsymbol{M}^{(2)}\end{bmatrix}}_{=\boldsymbol{M}}\begin{bmatrix}\ddot{\boldsymbol{x}}^{(1)}\\ \ddot{\boldsymbol{x}}^{(2)}\end{bmatrix}+\underbrace{\begin{bmatrix}\boldsymbol{K}^{(1)} & \boldsymbol{0}\\ \boldsymbol{0} & \boldsymbol{K}^{(2)}\end{bmatrix}}_{=\boldsymbol{K}}\begin{bmatrix}\boldsymbol{x}^{(1)}\\ \boldsymbol{x}^{(2)}\end{bmatrix}=\begin{bmatrix}\boldsymbol{B}_\mathsf{T}^{(1)}\\ \boldsymbol{B}_\mathsf{T}^{(2)}\end{bmatrix}\boldsymbol{F}_\mathsf{T}+\begin{bmatrix}\boldsymbol{B}_\mathsf{N}^{(1)}\\ \boldsymbol{B}_\mathsf{N}^{(2)}\end{bmatrix}\boldsymbol{F}_\mathsf{N}+\begin{bmatrix}\boldsymbol{F}^{(1)}\\ \boldsymbol{F}^{(2)}\end{bmatrix} \tag{2}$$

$$\dot{\boldsymbol{F}}_\mathsf{T}=\boldsymbol{f}(\boldsymbol{F}_\mathsf{T},{\boldsymbol{B}_\mathsf{T}^{(1)}}^\mathrm{T}\boldsymbol{x}^{(1)}-{\boldsymbol{B}_\mathsf{T}^{(2)}}^\mathrm{T}\boldsymbol{x}^{(2)},\boldsymbol{F}_\mathsf{N},\boldsymbol{\mu},\boldsymbol{c}_\mathsf{T}) \tag{3}$$

$$\boldsymbol{F}_\mathsf{N}=\boldsymbol{g}({\boldsymbol{B}_\mathsf{N}^{(1)}}^\mathrm{T}\boldsymbol{x}^{(1)}-{\boldsymbol{B}_\mathsf{N}^{(2)}}^\mathrm{T}\boldsymbol{x}^{(2)},\boldsymbol{c}_{\mathsf{N},\boldsymbol{0}},\boldsymbol{c}_{\mathsf{N},\boldsymbol{1}}), \tag{4}$$

where the system matrices are partitioned according to the DOFs of substructure 1 and substructure 2.

For the friction, a 2-D elastic–plastic model (or Jenkins element) is chosen. A nonlinear stiffness relationship is used for the contact law Fig. 2. Please note that Eq. 2 is a general representation valid for a broad class of friction and contact models although the special properties of the applied friction model are later exploited in the numerical implementation.

2.1 Craig-Bampton Method

The Craig-Bampton method [4] is shortly presented starting from the structural dynamics of a linear substructure k,

$$\boldsymbol{M}\,\ddot{\boldsymbol{x}}+\boldsymbol{K}\,\boldsymbol{x}=\boldsymbol{F}, \tag{5}$$

which is partitioned into free (inner) and interface DOFs. All quantities are related to the substructure k, the index is omitted for brevity. The DOFs are transformed to interface and relative coordinates by

$$\begin{bmatrix}\boldsymbol{x}_\mathsf{f}\\ \boldsymbol{x}_\mathsf{i}\end{bmatrix}=\begin{bmatrix}\boldsymbol{I} & -\boldsymbol{K}_\mathsf{ff}^{-1}\boldsymbol{K}_\mathsf{fi}\\ \boldsymbol{0} & \boldsymbol{I}\end{bmatrix}\begin{bmatrix}\boldsymbol{x}_\mathsf{r}\\ \boldsymbol{x}_\mathsf{i}\end{bmatrix}. \tag{6}$$

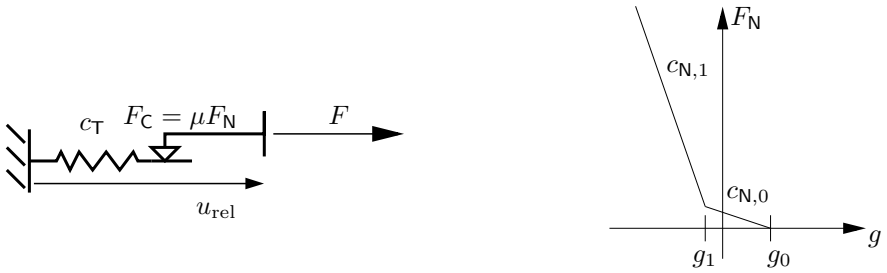

Figure 2: Left: Elasto–plastic friction model (shown for 1-D case); Right: Nonlinear contact law in normal direction.

The key is the reduction of relative coordinates $\boldsymbol{x}_\mathsf{r}$, whereas the interface DOFs are kept as physical coordinates. The eigenvalue problem

$$\boldsymbol{M}_{\mathsf{ff}}\ddot{\boldsymbol{x}}_\mathsf{r} + \boldsymbol{K}_{\mathsf{ff}}\boldsymbol{x}_\mathsf{r} = 0 \tag{7}$$

gives the first m_r fixed interface modes stacked in the modal base $\boldsymbol{\Theta}_\mathsf{r}$. Thereby, the choice of the number m_r of retained modes depends on the desired dynamic bandwidth for which accuracy is demanded. Finally, it follows

$$\begin{bmatrix}\boldsymbol{x}_\mathsf{f}\\ \boldsymbol{x}_\mathsf{i}\end{bmatrix} = \begin{bmatrix}\boldsymbol{\Theta}_\mathsf{r} & -\boldsymbol{K}_{\mathsf{ff}}^{-1}\boldsymbol{K}_{\mathsf{fi}}\\ \boldsymbol{0} & \boldsymbol{I}\end{bmatrix}\begin{bmatrix}\boldsymbol{x}_\mathsf{m}\\ \boldsymbol{x}_\mathsf{i}\end{bmatrix} = \underbrace{[\boldsymbol{\Theta}_{\mathsf{IM}}\,\boldsymbol{\Theta}_{\mathsf{CM}}]}_{=\boldsymbol{\Theta}}\begin{bmatrix}\boldsymbol{x}_\mathsf{m}\\ \boldsymbol{x}_\mathsf{i}\end{bmatrix}. \tag{8}$$

The modal base consists of two parts, the fixed–interface modes $\boldsymbol{\Theta}_{\mathsf{IM}}$ and the constraint modes $\boldsymbol{\Theta}_{\mathsf{CM}}$, which are the static solution for unit displacement of each individual interface DOF when the other interface DOFs are fixed. The reduced mass and stiffness matrices are found by projection of the system matrices on the reduction base according to

$$\hat{\boldsymbol{K}} = \boldsymbol{\Theta}^{\mathrm{T}}\boldsymbol{K}\boldsymbol{\Theta},\ \hat{\boldsymbol{M}} = \boldsymbol{\Theta}^{\mathrm{T}}\boldsymbol{M}\boldsymbol{\Theta}. \tag{9}$$

The obtained reduced matrices are dense matrices whereas the original matrices are sparse. This reduction is performed for each substructure $k = \{1, 2\}$ individually, where the interface DOFs are the DOFs of the joint interface of the substructure. The reduced matrices can be calculated for each substructure independently, i.e. the overall system matrices become block–diagonal. Because of the similarity of the assembly step to the FE method, the reduced substructures can also be seen as superelements.

2.2 Craig–Bampton Reduction Approach with Common Interface Reduction (Method A)

For further order reduction, the found constraint mode bases are reduced. This approach is extended in a novel way in the following, where the interface DOF reduction is conducted for the overall structure in one step. This allows to reduce all substructures by the standard Craig–Bampton method first and then the interface DOFs when the overall structure model is assembled. It has the advantage that the number of retained interface DOFs are distributed between the separate substructures in an optimal sense.

Each reduction base $\boldsymbol{\Theta}^{(k)}$ consists of a normal mode base $\boldsymbol{\Theta}_{\mathsf{NM}}^{(k)}$ and a constraint mode base $\boldsymbol{\Theta}_{\mathsf{CM}}^{(k)}$, i.e.

$$\boldsymbol{\Theta}^{(k)} = [\boldsymbol{\Theta}_{\mathsf{NM}}^{(k)},\, \boldsymbol{\Theta}_{\mathsf{CM}}^{(k)}]. \tag{10}$$

Fixed–interface modes are used following the Craig–Bampton approach, i.e. $\boldsymbol{\Theta}_{\mathsf{NM}} = \boldsymbol{\Theta}_{\mathsf{IM}}$. A static condensation on the joint interface DOFs is performed for both interfaces by using

$$\boldsymbol{\Theta}_\mathsf{s} = \begin{bmatrix}\boldsymbol{\Theta}_{\mathsf{CM}}^{(1)} & \boldsymbol{0}\\ \boldsymbol{0} & \boldsymbol{\Theta}_{\mathsf{CM}}^{(2)}\end{bmatrix}. \tag{11}$$

which gives the reduced system matrices

$$\hat{\boldsymbol{M}} = \boldsymbol{\Theta}_\mathsf{s}^{\mathrm{T}}\begin{bmatrix}\boldsymbol{M}^{(1)} & \boldsymbol{0}\\ \boldsymbol{0} & \boldsymbol{M}^{(2)}\end{bmatrix}\boldsymbol{\Theta}_\mathsf{s} \ \text{ and } \ \hat{\boldsymbol{K}} = \boldsymbol{\Theta}_\mathsf{s}^{\mathrm{T}}\begin{bmatrix}\boldsymbol{K}^{(1)} & \boldsymbol{0}\\ \boldsymbol{0} & \boldsymbol{K}^{(2)}\end{bmatrix}\boldsymbol{\Theta}_\mathsf{s}. \tag{12}$$

Now, a reduced eigenvalue problem on the interface is formulated,

$$\left(\hat{\boldsymbol{K}} - \omega^2\hat{\boldsymbol{M}}\right)\boldsymbol{\psi} = \boldsymbol{0}, \tag{13}$$

and solved for the desired number m_i of eigenvectors for the overall structure. Expansion to the substructure DOF vectors yields the reduced constraint–mode base $\boldsymbol{\Theta}^*_{\mathsf{CM}}$ that is combined with normal mode base of the overall structure,

$$\boldsymbol{\Theta} = [\boldsymbol{\Theta}_{\mathsf{NM}},\, \boldsymbol{\Theta}^*_{\mathsf{CM}}]. \tag{14}$$

Then, the common reduction base $\boldsymbol{\Theta}$ is applied to the mass and stiffness matrices, i.e.

$$\hat{\boldsymbol{M}} = \boldsymbol{\Theta}^{\mathrm{T}} \begin{bmatrix} \boldsymbol{M}^{(1)} & \boldsymbol{0} \\ \boldsymbol{0} & \boldsymbol{M}^{(2)} \end{bmatrix} \boldsymbol{\Theta} \;\text{ and }\; \boldsymbol{hatK} = \boldsymbol{\Theta}^{\mathrm{T}} \begin{bmatrix} \boldsymbol{K}^{(1)} & \boldsymbol{0} \\ \boldsymbol{0} & \boldsymbol{K}^{(2)} \end{bmatrix} \boldsymbol{\Theta}. \tag{15}$$

2.3 Free–Interface Reduction Approach with Reduced Set of Joint Constrained Interface Modes (Method B)

The following reduction methodology is motivated by a publication of [18] where the law of actio and reaction at the joint interface is exploited in order to introduce Joint Interface Modes. This is now applied to systems with friction for the first time for the knowledge of the authors.

Starting again from the structural dynamics of the linear substructure k, free interface modes are calculated by the eigenvalue problem

$$\left(\boldsymbol{K}^{(k)} - \omega^2 \boldsymbol{M}^{(k)}\right) \boldsymbol{\psi} = \boldsymbol{0}. \tag{16}$$

Then, a modal base is constructed by the combination of the m free interface normal modes with the lowest eigenfrequencies to capture the system dynamics, $\boldsymbol{\Theta}^{(k)}_{\mathsf{NM}}$, and the constraint modes $\boldsymbol{\Theta}^{(k)}_{\mathsf{CM}}$ from Eq. 8. After static condensation on the interface DOFs similar to Eq. 12, the obtained system is additionally partitioned with respect to the substructures of the joint DOFs. This gives the reduced local system

$$\begin{bmatrix} \hat{\boldsymbol{M}}^{(11)}_{\mathsf{i}} & \hat{\boldsymbol{M}}^{(12)}_{\mathsf{i}} \\ \hat{\boldsymbol{M}}^{(12)^{\mathrm{T}}}_{\mathsf{i}} & \hat{\boldsymbol{M}}^{(22)}_{\mathsf{i}} \end{bmatrix} \begin{bmatrix} \ddot{\boldsymbol{x}}^{(1)}_{\mathsf{i}} \\ \ddot{\boldsymbol{x}}^{(2)}_{\mathsf{i}} \end{bmatrix} + \begin{bmatrix} \hat{\boldsymbol{K}}^{(11)}_{\mathsf{i}} & \hat{\boldsymbol{K}}^{(12)}_{\mathsf{i}} \\ \hat{\boldsymbol{K}}^{(12)^{T}}_{\mathsf{i}} & \hat{\boldsymbol{K}}^{(22)}_{\mathsf{i}} \end{bmatrix} \begin{bmatrix} \boldsymbol{x}^{(1)}_{\mathsf{i}} \\ \boldsymbol{x}^{(2)}_{\mathsf{i}} \end{bmatrix} = \begin{bmatrix} \boldsymbol{F}^{(1)}_{\mathsf{i}} \\ \boldsymbol{F}^{(2)}_{\mathsf{i}} \end{bmatrix} = \begin{bmatrix} \boldsymbol{F}^{(1)}_{\mathsf{i}} \\ -\boldsymbol{F}^{(1)}_{\mathsf{i}} \end{bmatrix}. \tag{17}$$

If the friction interface is located between two completely separated substructures in this work, the coupling matrices evaluate to zero (this important property is not mentioned in [18]), i.e.

$$\hat{\boldsymbol{M}}^{(12)}_{\mathsf{i}} = 0,\, \hat{\boldsymbol{K}}^{(12)}_{\mathsf{i}} = 0. \tag{18}$$

Neglection of the inertia effects in Eq. 17 allows to express $\boldsymbol{x}^{(1)}_{\mathsf{i}}$ by $\boldsymbol{x}^{(2)}_{\mathsf{i}}$

$$\boldsymbol{x}^{(1)}_{\mathsf{i}} = \underbrace{-\left(\hat{\boldsymbol{K}}^{(11)}_{\mathsf{i}} + \hat{\boldsymbol{K}}^{(12)}_{\mathsf{i}}\right)^{-1} \left(\hat{\boldsymbol{K}}^{(22)}_{\mathsf{i}} + \hat{\boldsymbol{K}}^{(12)^{\mathrm{T}}}_{\mathsf{i}}\right)}_{=\boldsymbol{G}} \boldsymbol{x}^{(2)}_{\mathsf{i}}, \tag{19}$$

which is plugged back into Eq. 17. The obtained modified reduced local system dynamics leads again to an eigenvalue problem,

$$\left(\hat{\boldsymbol{K}} - \omega^2 \hat{\boldsymbol{M}}\right) \boldsymbol{\psi} = \boldsymbol{0}, \tag{20}$$

which is solved for the desired number m_j of lowest eigenvectors for the overall structure. Expansion of this vectors to the substructure DOF vector gives the reduced constraint–mode bases for m_j joint interface modes,

$$\boldsymbol{\Theta}^{(2)^*}_{\mathsf{CM}} = \begin{bmatrix} -\hat{\boldsymbol{K}}^{(2)^{-1}}_{\mathsf{ff}} \hat{\boldsymbol{K}}^{(1)}_{\mathsf{fi}} \\ \boldsymbol{I} \end{bmatrix} \underbrace{\left[\hat{\boldsymbol{\psi}}_1, \ldots, \hat{\boldsymbol{\psi}}_{m_\mathsf{j}}\right]}_{=\hat{\boldsymbol{\Theta}}_\mathsf{i}},\; \boldsymbol{\Theta}^{(1)^*}_{\mathsf{CM}} = \begin{bmatrix} -\hat{\boldsymbol{K}}^{(1)^{-1}}_{\mathsf{ff}} \hat{\boldsymbol{K}}^{(1)}_{\mathsf{fi}} \boldsymbol{G} \\ \boldsymbol{G} \end{bmatrix} \hat{\boldsymbol{\Theta}}_\mathsf{i}. \tag{21}$$

Finally, the derived base $\boldsymbol{\Theta}_{\mathsf{IM}}$ is added to the reduction base according to Eq. 10,

$$\boldsymbol{\Theta} = \begin{bmatrix} \boldsymbol{\Theta}^{(1)}_{\mathsf{NM}} & \boldsymbol{0} & \boldsymbol{\Theta}^{(1)^*}_{\mathsf{CM}} \\ \boldsymbol{0} & \boldsymbol{\Theta}^{(2)}_{\mathsf{NM}} & \boldsymbol{\Theta}^{(2)^*}_{\mathsf{CM}} \end{bmatrix}. \tag{22}$$

Additional static attachment modes may be added to the reduction base. Following the idea that any representative vectors can be used as Ritz vectors, this can be further generalized such that nonlinear full–order model static solutions are added to achieve excellent static solution prediction as it is later done.

3 Application: Prediction of Friction Damping by Transient Simulations

For linear structures, the main criteria in the application of model reduction and substructuring methods is the accurate prediction of eigenfrequencies and eigenvectors whereas the prediction of damping in joints additionally demands accurate prediction of the normal pressure. Hence, the error of the contact pressure should be specifically evaluated in order to make sure that correct damping prediction is possible.

3.1 Investigated Test Structure

A beam with attached friction damper (see Tab. 2 for dimensions and Fig. 3 for FE mesh) is used to investigate the proposed reduction methods. The bolts are modelled as discrete masses connected by shaft stiffnesses. The imposed pretension by the tightened screws is captured by special pretension elements.

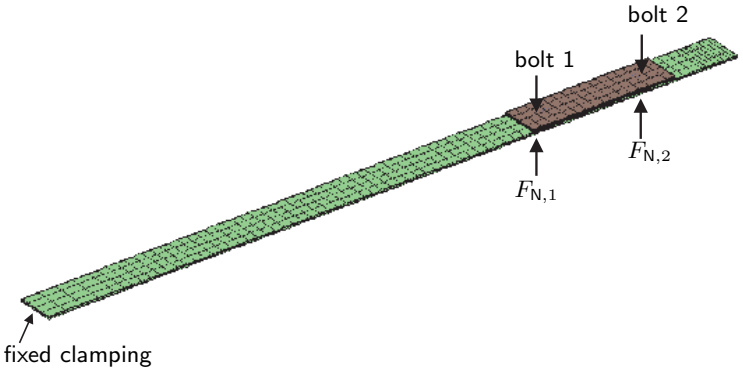

Figure 3: FE mesh of test structure used for model reduction.

Table 2: Material and geometric properties of the investigated structure.

Parameter	*Beam structure*	*Friction damper*
length	775 mm	160 mm
width	40 mm	40 mm
Thickness	3 mm	3 mm
material	steel	steel
Young's modulus	205 GPa	205 GPa
Poisson's ratio	0.3	0.3
density	8000 kg/m^3	8000 kg/m^3

3.2 Convergence of the Static Solution

For all considered reduction methods, the static convergence behavior is investigated as a preliminary for accurate damping prediction. Specifically, the convergence of the reduced model solution to the exact full order solution with increasing number of retained generalized interface DOFs is evaluated. For that, all static loads are applied, i.e. the bolt pretension is modelled by prescribed normal forces $F_{\mathrm{N},1}$ and $F_{\mathrm{N},2}$.

If the strain energy norm is applied, the relative error is defined for the reduced model static solution $\boldsymbol{u}$ with respect to the strain energy E composed of the linear parts and the contact and friction contributions

$$e_{\mathrm{strain}} = \frac{E - E_{\mathrm{ref}}}{E_{\mathrm{ref}}}. \tag{23}$$

It is calculated for each reduction method and a fixed number of normal modes for an increasing number of retained generalized interface DOFs, i.e. decreasing reduction level of the constraint modes. For this comparison, no additional static attachment modes are used. As seen in Fig. 4, strictly monotonic behavior is observed as expected and both methods show good convergence, although method B yields superior convergence for small DOF numbers in terms of all

investigated error norms. For accurate damping prediction, the relative normal displacement error in the contact area is very important. Hence, the contact gap error is visualized for two example reduction degrees in Fig. 5 for method B. For higher accuracy of the reduced solution, the error is more equally distributed on the contact interface. Furthermore, due to the symmetry of the problem, the error profile is also symmetric.

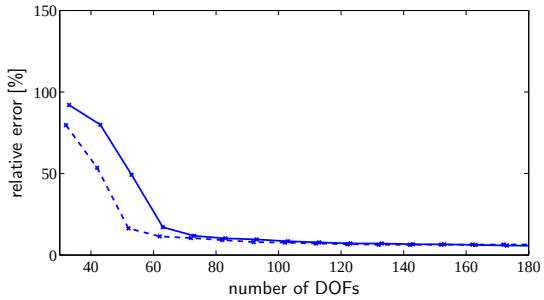

Figure 4: Comparison of the static strain energy norm error e_{strain} (Eq. 23) for increasing number of (generalized) interface DOFs for method A (—) and method B (– – –).

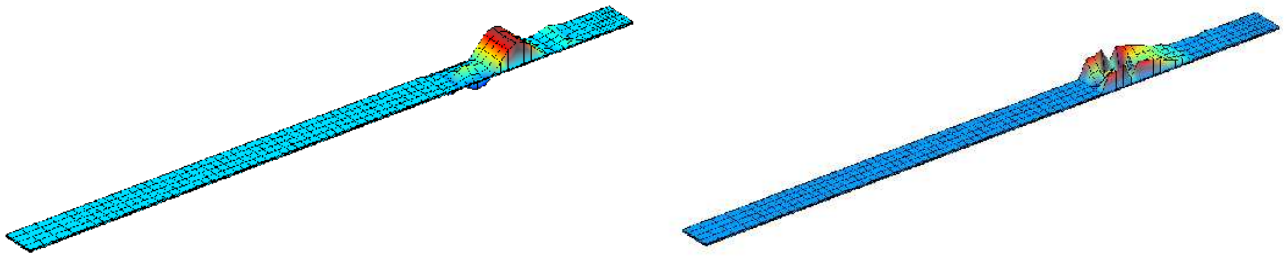

(a) 147 % relative gap error (42 interface DOFs)

(b) 2.9 % relative gap error (102 interface DOFs)

Figure 5: Absolute gap error $\boldsymbol{g} - \boldsymbol{g}_{\text{ref}}$ (individually normalized) visualized as vertical displacements on the contact area of the FE model of the beam substructure (damper not shown, displacements outside of contact surface are set to 0).

3.3 Frequency Response Functions (FRF)

A set of accelerance frequency response functions (FRF) obtained from simulations of the exact full order model and of the reduced models are compared in Figs. 6 and 7. The reduction method A is the Craig–Bampton method with interface reduction for the whole structure with the exact nonlinear static solution added as additional attachment mode to the modal base. Method B is based on the free interface reduction approach with joint interface mode reduction. As in method A, the exact nonlinear solution is added as an attachment mode. The FRFs are calculated from simulated transient responses of 2 s for experimentally measured impulse force excitation signals. In order to avoid leakage effects, an exponential window of 1 s time constant is applied. Normal forces $F_{\text{N},1}$ of 333 N, 667 N and 1000 N are applied to the variable screw at bolted joint 1 whereas the other screw is fixed by a normal force $F_{\text{N},2} = 4000$ N. Example results for the two methods compared to the exact solution are presented in Figs. 6 and 7. For comparable results, the method A needs 71 DOFs whereas the method B only needs 56 DOFs for the same or even better prediction accuracy, which is contributed to the faster convergence of the constraint mode reduction — see Fig. 4.

The plots and the calculated errors show that the eigenfrequencies, the peak heights and widths (which are important for the damping prediction) as well as the transfer zeros are very well matched by the reduced models.

3.4 Evaluation of Computation Time Reduction

In transient simulations of nonlinear systems, the number of DOFs has a strong impact on the computation time because nonlinear equilibrium iterations with updated tangential matrices must be performed at every time step. The nonlinear

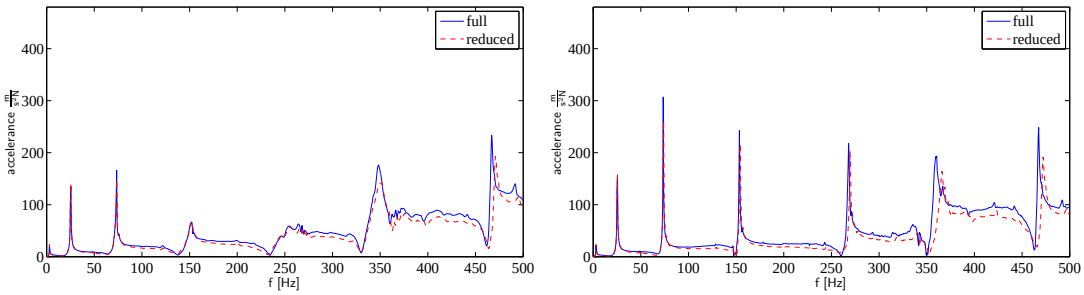

(a) $F_{\mathrm{N},1} = 333$ N (b) $F_{\mathrm{N},1} = 1000$ N

Figure 6: Impulse FRFs for method A for different normal forces (note the linear scale).

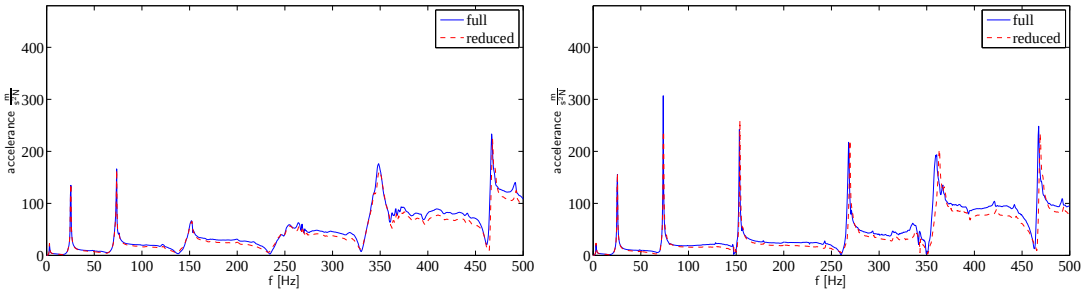

(a) $F_{\mathrm{N},1} = 333$ N (b) $F_{\mathrm{N},1} = 1000$ N

Figure 7: Impulse FRFs for method B for different normal forces (note the linear scale).

Newmark time integration scheme with Newton–Raphson iterations is applied using consistent tangential matrices. These iterations lead to very high computational costs which makes – in contrast to other CMS applications – the initial effort to calculate the reduction base and to reduce the matrices vanish in the overall necessary effort for the analysis.

The found computation times for transient simulations of the full and differently reduced models are listed in Tab. 3 where the standard Craig–Bampton method without interface reduction step, the improved Craig–Bampton method A and the free–interface method B are compared to the original full model. In order to assess the required computation time, the ratio of necessary CPU time to simulation time is determined. Additionally, the found ratios are set in relation to the full order solution to obtain the improvement factors. For comparison reasons, the computation time for the full model with the commercial FE code ANSYS is given (using Newmark scheme and a line search algorithm). In view that its algorithms are implemented in a low–level programming language better optimized to the computer platforms in contrast to the MATLAB implementation of the presented solutions, i.e. in a high–level script programming language, the performance of the full order solution is considered very good. Please note that ANSYS does not give detailed insight and control over the implemented algorithms, i.e. it is a somewhat black–box solution.

Both presented reduction methods yield excellent accuracy and hereby make a complete analysis on a standard PC feasible. For the considered scenario, one sensible analysis consists of a transient simulation of $t_{\mathrm{sim}} = 6$ s which takes either 71 min or 42 min, depending on the chosen reduction method. For the full model, this would take about 193 hours which explains why a simulation time of 2 s is chosen for the comparisons of the last section. The computation time for the reduced standard Craig–Bampton model is found to be rather high because the reduction of the number of DOFs is compensated by the extra effort for the dense system matrices.

3.5 Simulation and Analysis Framework

A simulation and analysis framework shown in Fig. 8 has been developed that is capable to use linear substructure models from commercial FE codes. The substructures may be additionally moved in space and are then assembled with the zero–thickness elements implementing the contact and friction effects on the defined contact areas in an assembly step. Furthermore, reduction methods may be applied to the built overall structural dynamics or individual parts of it. Static and transient solvers are implemented for both full–order and reduced models and the results can be post–processed. One typical way of post–processing is to calculate frequency response function (FRF) and to estimate the modal parameters or to export the FRFs to commercial post–processing tools for special analysis.

Table 3: Computation times for different reduction methods and reduced model sizes for transient simulation of an impulse response. The given values are pure CPU times on a single CPU of a standard PC (3 GHz Intel Xeon/Core 5160).

Reduction method	DOFs	Ratio $t_{\text{cpu}}/t_{\text{sim}}$	Improvement factor
full model (reference)	5955	36699	1.0
ANSYS (full model)	5955	90499	2.5
standard Craig–Bampton	533	73530	2.0
method A	73	709	51.8
method B	52	422	87.0

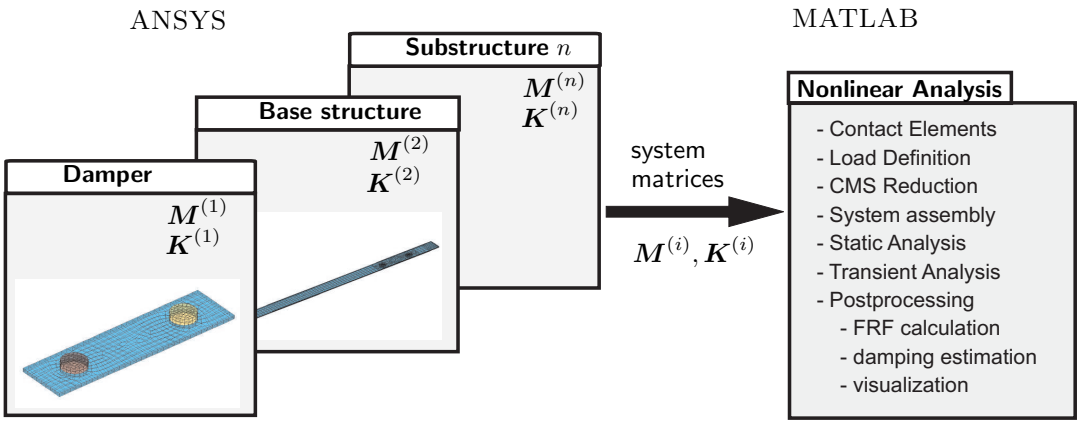

Figure 8: Simulation framework for nonlinear structural analysis of mechanical structures with friction.

4 Experimental Verification

The developed efficient simulation framework employing model reduction is a key tool in order to perform model updating or parameter variations on a standard PC. In the sequel, results from such an updating procedure of a FE model to experimental data are presented. For similar material parameters as given before in Tab. 2 for the model in Fig. 3, a refined FE model is used as shown in Fig. 9. Compared to the reduction test model, the bolts and holes are now modelled and the discretization is refined close to the bolts where high normal pressures appear. The FE model has now 21564 DOFs (603 pairs of contact nodes) and is reduced to 57 DOFs.

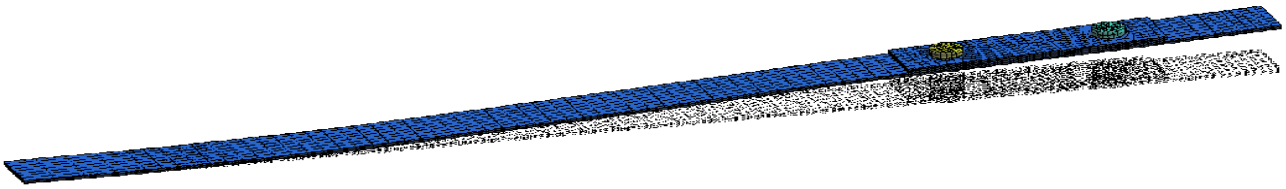

Figure 9: Mesh of investigated structure with attached friction damper (example deformation and undeformed reference).

4.1 Model Updating

For model updating, so–called linearizing excitation signals are employed because they yield linearized FRFs, i.e. FRFs resembling those obtained from linear systems [19]. Although random excitation is found to be best linearizing in experiments, deterministic impulse excitation is chosen because the necessary simulation time for random excitation would be very large. In the experimental setup, the excitation is applied by an impulse hammer close to the tip and the responses are measured at several points on the structure. The shown driving point FRFs are calculated from the measured acceleration on the opposite surface. Excitation is located on the mid–line of the beam, hence virtually no torsional modes are excited. Measurements are conducted for a set of different normal forces $F_{\text{N},1}$ whereas the normal force at the other damper end is

Table 4: Found contact parameters for best match of simulation with experiment.

Parameter	Variable	Value
friction coefficient	μ	0.2
normal stiffnesses	$c_{\mathrm{N},0}$, $c_{\mathrm{N},1}$	$3.87 \cdot 10^{11}\ \frac{N}{m^3}$, $7.74 \cdot 10^{11}\ \frac{N}{m^3}$
gap distances	g_0, g_1	$-5 \cdot 10^{-7}$ m, 0 m
tangential stiffness	c_{T}	$7.74 \cdot 10^{11}\ \frac{N}{m^3}$

again constantly set to $F_{\mathrm{N},2} = 4000$. An exponential window of 2 s time constant is applied before the FRFs are calculated from five individual measurements averaged in frequency domain.

For the simulations, experimentally measured impulses are averaged and applied as loads. As in the measurements, FRFs are calculated from the 6 s responses using an exponential window of time constant $\tau = 2$ s. Classical Rayleigh damping is assumed with parameters determined from experimental modal analysis of the base structure. In the model updating, the friction coefficient, the tangential contact stiffness and the normal contact stiffness are varied in a systematic way to match the experimental data to find the best match parameter set given in Tab. 4. For this parameters, the simulated and the measured FRFs are compared in Fig. 10. Obviously, the chosen excitation force with roughly 100 N peak force significantly excites higher harmonics of the system. Simulations have proven that they are mostly due to the normal contact between damper and base structure. Due to internal resonances, the amplitudes of these higher harmonics depend on their frequencies in relation to the resonance frequencies of the structure as well as on the spatial location of the friction and contact interface which makes them not predictable by analytical means. The qualitative shape of the resonance peaks, the width and height determining the damping and the locations of the higher harmonics are very well predicted by the simulations. Obviously, a very good match quality is observed for all measured normal force cases between $F_{\mathrm{N},1} = 13$ and $F_{\mathrm{N},1} = 1000$ N. Further results, presented in Fig. 11, show the effects of a higher friction coefficient of $\mu = 0.4$.

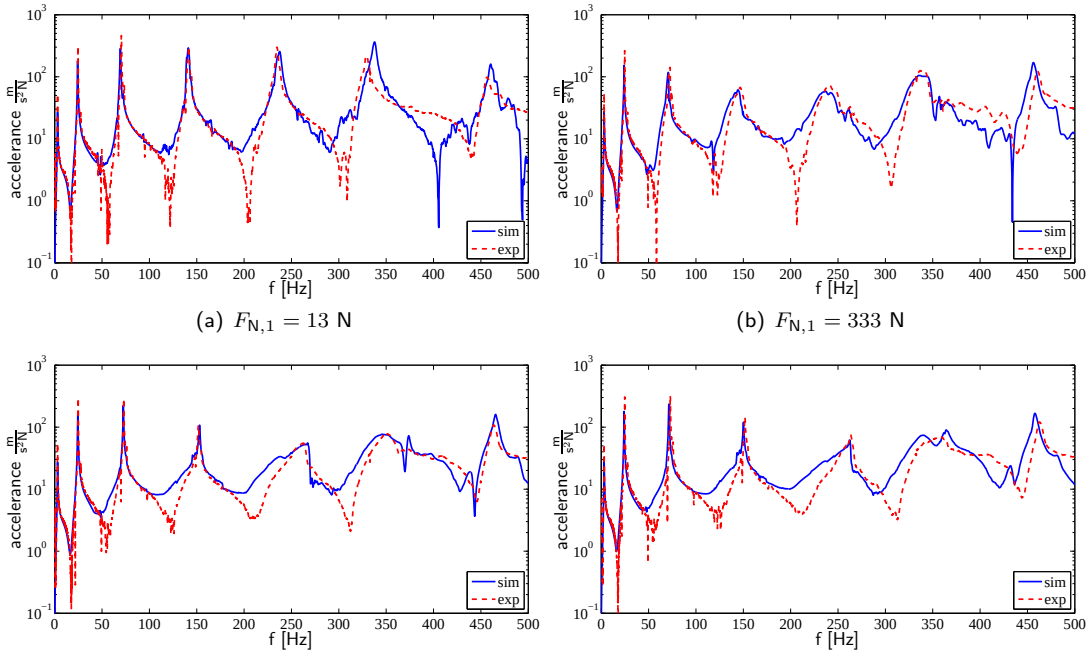

(a) $F_{\mathrm{N},1} = 13$ N (b) $F_{\mathrm{N},1} = 333$ N

(c) $F_{\mathrm{N},1} = 667$ N (d) $F_{\mathrm{N},1} = 1000$ N

Figure 10: Comparison of measured and simulated FRFs for best match parameter case (cf. Tab. 4).

4.2 Evaluation of Modal Damping

Although friction is a nonlinear effect, there is a big interest in evaluating the damping effect in terms of modal damping ratios known from linear structural dynamics. This is mainly because modal damping ratios can easily be measured and

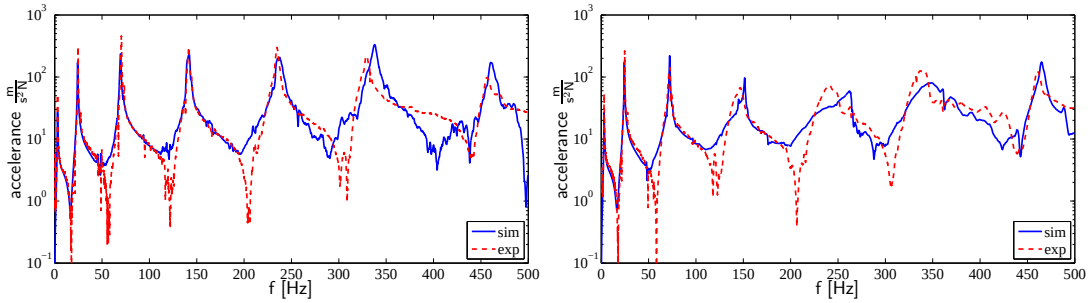

(a) $F_{\mathrm{N},1} = 13$ N (b) $F_{\mathrm{N},1} = 333$ N

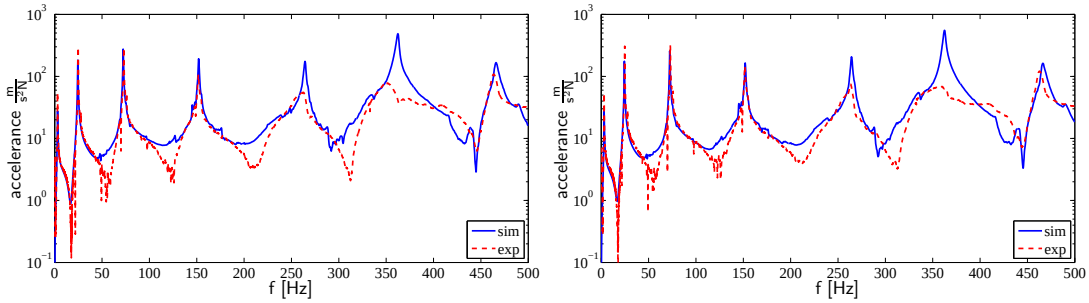

(c) $F_{\mathrm{N},1} = 667$ N (d) $F_{\mathrm{N},1} = 1000$ N

Figure 11: Comparison of measured and simulated FRFs for with varied friction coefficient $\mu = 0.4$.

compared in engineering practice. For evaluation of modal damping for nonlinear structures – in contrast to linear structures – the excitation type and amplitude must be controlled for fair comparisons and correct analysis. The modal damping ratios are determined by the 3dB–bandwidth method from the FRFs [5]. As mentioned before, an exponential window is applied to the simulated or measured acceleration responses to prevent leakage. For the chosen exponential window with time constant τ, the artifical damping δ_k^{win} added to the apparent modal damping δ_k^{det} of mode k can be compensated for (under the assumption of linear dynamics) [5], i.e. $\delta_k = \delta_k^{\mathrm{det}} - \delta_k^{\mathrm{win}}$ with $\delta_k^{\mathrm{win}} = 1/(2\ \tau\omega_k)$.

The modal damping ratios δ_k from simulations and experiments are compared in Fig. 12, where excellent agreement is observed. The numerically predicted modal dampings match the experimental ones quite well, especially if one keeps in mind, that measurement errors influence much more the damping identification than the eigenfrequency identification. The variations in the damping of mode 1 is most probably due to the high constribution of artifical window damping and violation of the linear dynamics assumption for the physical damping recovery. As expected, the corresponding eigenfrequencies and the found damping ratios strongly dependent on the applied normal forces.

5 Conclusions

The usefulness of CMS methods applied to the simulation of mechanical structures with friction and joints has been demonstrated, by which parameter updating has become feasible for a real–world structure on a single standard PC. Excellent agreement between the simulated and measured FRFs shows that the inclusion of friction in the design process allows to predict its influence on damping and eigenfrequencies as well as the generation of higher harmonics. As a strong advantage, the output variables of interest need not to be known before the reduction step, because the full displacement vector is recovered from the reduced solution. Furthermore, the applied substructuring approach allows to efficiently assemble and quickly analyse different configurations made up from different combinations of substructures if the substructures can be reduced once and saved in a database.

The development of own static and transient solvers offers the possibility to investigate various modifications of the contact model, to relatively easily incorporate it into optimization procedures or to simulate a feedback controllers, that in general can not be implemented in commercial FE codes in a straight way.

Currently, semi–analytical methods such as the harmonic balance method are investigated to directly obtain results in the frequency domain. Further work may focus on optimization of the implementation and on applications of the presented methodology to more complex structures or in industrial applications.

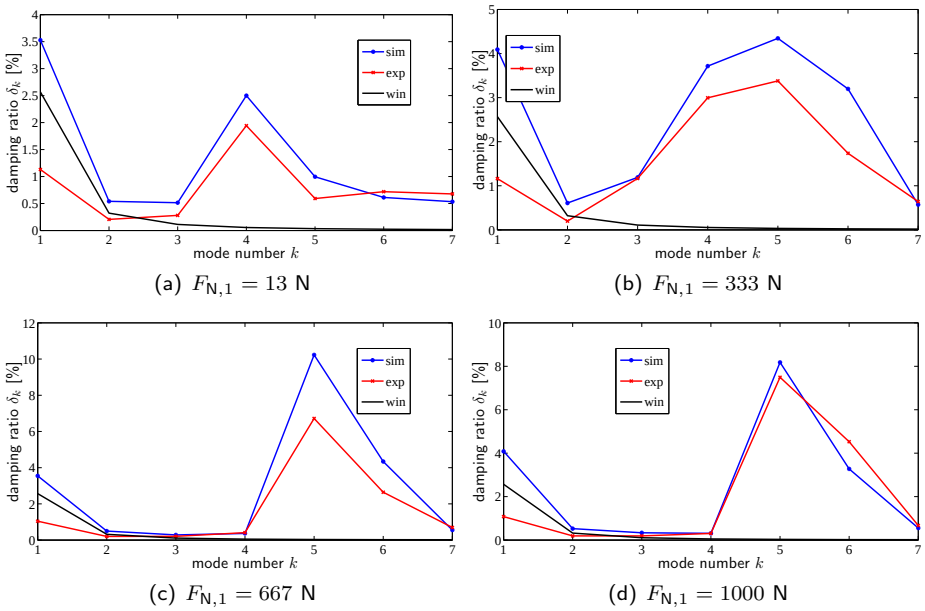

(a) $F_{\mathrm{N},1} = 13$ N (b) $F_{\mathrm{N},1} = 333$ N

(c) $F_{\mathrm{N},1} = 667$ N (d) $F_{\mathrm{N},1} = 1000$ N

Figure 12: Modal damping ratios δ_k from simulation and experiment (artificial window damping shown for information).

Acknowledgment

The support of the DFG (German Research Foundation) by the project SPP 1156 is grateful acknowledged.

References

[1] Ahmadian, H., Mottershead, J. E., James, S., Friswell, M., and Reece, C. Modelling and updating of large surface-to-surface joints in AWE-MACE structure. *Mechanical Systems and Signal Processing 20* (2006), 868–880.

[2] Becker, J., and Gaul, L. Semi-active control of adaptive friction dampers for structural vibration control. In *Proceedings of the IMAC-XXV: A Conference & Exposition on Structural Dynamics* (Orlando, Florida USA, 2007).

[3] Craig, R. R. A brief tutorial on substructure analysis and testing. In *Proceedings of IMAC XVIII* (2000).

[4] Craig, R. J., and Bampton, M. C. C. Coupling of substructures for dynamic analysis. *AIAA Journal 6*, 7 (1968), 1313–1319.

[5] Ewins, D. J. *Modal Testing: Theory and Practice*. John Wiley & Sons Inc., New York, 1984.

[6] Gaul, L. Wave transmission and energy dissipation at structural and machine joints. *Journal of Vibration, Acoustics, Stress, and Reliability in Design 105* (1983), 489–496.

[7] Gaul, L. The influence of damping on waves and vibrations. *Mechanical Systems and Signal Processing 13*, 1 (1999), 1–30.

[8] Gaul, L., Albrecht, H., and Wirnitzer, J. Semi-active friction damping of large space truss structures. *Journal of Shock and Vibration 11* (2004), 173–186.

[9] Jalali, H., Ahmadian, H., and Mottershead, J. E. Identification of bolted lap joints parameters in assembled structures. *International Journal of Solids and Structures submitted* (2007).

[10] Kappagantu, R. V., and Feeny, B. F. Part 1: Dynamical characterization of a frictionally excited beam. *Nonlinear Dynamics 22*, 4 (2000), 317–333.

[11] Kappagantu, R. V., and Feeny, B. F. Part 2: Proper orthogonal modal modeling of a frictionally excited beam. *Nonlinear Dynamics 23*, 1 (2000), 1–11.

[12] Mayer, M., and Gaul, L. Segment-to-segment contact elements for modelling joint interfaces in finite element analysis. *Mechanical Systems and Signal Processing 21*, 2 (Feb. 2007), 724–734.

[13] Menq, C. H., Griffin, J. H., and Bielak, J. The influence of microslip on vibratory response, part II: A comparison with experimental results. *Journal of Sound and Vibration 107*, 2 (June 1986), 295–307.

[14] Popp, K. Nichtlineare Schwingungen mechanischer Strukturen mit Füge- oder Kontaktstellen. *74*, 3 (1994), 147–165.

[15] Qu, Z.-Q. Model reduction for dynamical systems with local nonlinearities. *AIAA Journal 40*, 2 (2002), 327–333.

[16] Segalman, D. J. Model reduction of systems with localized nonlinearities. *J. Comput. Nonlinear Dynam. 2*, 3 (July 2007), 249–266.

[17] Wentzel, H., and Olsson, M. Numerical prediction of damping in structures with frictional joints. *International Journal of Vehicle Noise and Vibration 2*, 2 (2006), 125 – 142.

[18] Witteveen, W., and Irschik, H. Efficient modal formulation for vibration analysis of solid structures with bolted joints. In *Proceedings of IMAC XXV, Orlando, USA* (2007).

[19] Worden, K., and Tomlinson, G. R. *Nonlinearity in Structural Dynamics*. Insitute of Physics Publishing, 2001.